Revised manuscript (unmarked, editable source file) Click here to view linked References

Competing energy absorption and shape recovery in 3D-printed composite meta-honeycombs under cyclic compression

Peng-Xu Lu [a, b], James Dear [c], Clare Burnett [d], Zhongwei Guan [a], Zafer Kazancı [d], Jin Zhou [a, *], John P. Dear [c]

[a] *School of Mechanical Engineering, Xi'an Jiaotong University, Xi'an 710049, China*

[b] *Department of Bioresource Engineering, McGill University, Montreal, QC H9X 3V9, Canada*

[c] *Department of Mechanical Engineering, Imperial, London, SW7 2AZ, UK*

[d] *Advanced Composites Research Group, School of Mechanical and Aerospace Engineering, Queen's University Belfast, Belfast, BT9 5AH, UK*

**Corresponding E-mail: jin.zhou@xjtu.edu.cn (Jin Zhou)*

Abstract: This study investigates the cyclic compressive behavior of 3D-printed composite meta-honeycombs, focusing on the trade-off between energy absorption and shape recovery. Three configurations, hexagonal (HEX), auxetic re-entrant (ARE), and double arrow-head (DAH), were fabricated using Nylon and Onyx and tested under quasi-static cyclic compression in both in-plane and out-of-plane directions. Key metrics, including specific energy absorption (SEA), undulation of load-carrying capacity (ULC), shape recovery ratio (SRR), and energy dissipation ratio (EDR), were used to quantify repeatable energy absorption and recovery performance. Results reveal a pronounced competition between crashworthiness and recoverability. Fiber reinforcement enhances stiffness, strength, and SEA but reduces shape recovery, highlighting a material-level trade-off. SEA is generally higher under out-of-plane loading, while in-plane SRR is 25-35 % greater than the out-of-plane SRR, showing strong sensitivity to loading direction. Cyclic compression at different deformation stages leads to stage-dependent degradation, with SEA reductions of approximately 10 %, 50 %, and 100 % during the elastic, plateau, and densification stages, respectively. Finite element simulations elucidate configuration-dependent deformation mechanisms and support the experimental observations. This study establishes the universality of the trade-off across material systems, topologies, loading directions, cyclic stages, and provides quantitative insights for designing reusable energy-absorbing honeycomb structures.

Keywords: Meta-honeycombs; Cyclic compression; Energy absorption; Shape recovery; Chopped carbon fiber-reinforced composites.

1. Introduction

As a lightweight structure, honeycombs have been widely used in automotive, maritime and other civilian transport sectors, where their high specific strength, exceptional impact resistance and excellent crashworthiness are key benefits [1-3]. Owing to their ability to undergo progressive collapse and dissipate large amounts of energy at nearly constant stress levels, honeycombs have long been regarded as efficient energy absorbers for impact and crash protection applications [4, 5]. Considerable research efforts have therefore been devoted to tailoring honeycomb geometries, including triangular [6,

7], square [6, 8], hexagonal [9, 10], circular [11], re-entrant [12, 13], double V-shaped [14, 15], chiral [16, 17] and star-shaped [18, 19] configurations, to enhance their energy absorption performance under quasi-static and dynamic loading conditions.

With the rapid development of additive manufacturing technologies, particularly fused filament fabrication, increasing attention has been paid to 3D-printed composite honeycomb structures [20-22]. Sugiyama et al. [23] and Dou et al. [24] investigated the mechanical behavior of carbon fiber reinforced 3D printed honeycombs under a drop-weight impact, and compared it with traditional 3D printed honeycombs to explore the corresponding failure mechanism. Morales et al. [25] analyzed the influence of different cross sections on the crushing performance of 3D printed continuous carbon fiber reinforced tubes, and optimized the printing path. Using the 3D printing technology, Quan et al. [26], Zhao et al. [27] and Chikkanna et al. [28] fabricated auxetic honeycombs by carbon fiber reinforced polymers and conducted in-plane and out-of-plane compression tests on them to evaluate the crashworthiness. Zhou et al. [29] investigated the energy absorption of three different cellular honeycombs manufactured by chopped carbon fiber reinforced nylon and compared it with nylon honeycombs. From the aforementioned literatures, both chopped and continuous carbon-fiber-reinforced composites have been successfully utilized to fabricate architected honeycombs with improved stiffness, strength, and crashworthiness [30]. Besides, fiber reinforcement [31], printing path optimization [32], and unit-cell topology [33] can significantly enhance energy-absorbing capacity compared to unreinforced polymer honeycombs.

Beyond single-impact scenarios, many practical applications, such as reusable protective systems and impact mitigation components, require structures to sustain repeated loading events [34]. In such cases, energy absorption is insufficient to characterize structural performance. Instead, increasing attention has been directed toward the concept of repeatable energy absorption, which describes the ability of a structure to maintain meaningful energy-absorbing capability over multiple loading-unloading cycles despite accumulated damage and partial irreversibility [35]. Zeng et al. [36] and Cheng et al. [37] performed in-plane and out-of-plane quasi-static compression experiments on carbon fiber reinforced honeycombs with different geometric configurations, respectively. It was found that the shape recovery ratio of these honeycombs could reach up to 95 %, and the shape recoverability would be improved with the increase of fiber content. Ye et al. [38] presented a 3D printed continuous carbon fiber reinforced honeycomb with shape memory effect and carried out cyclic compression tests on it, which could be used to monitor the change of electrical resistance to sense the damage distribution in cyclic compression. Dong et al. [39] and Zeng et al. [40] evaluated the shape recovery ratio of carbon fiber reinforced honeycombs with electro- and thermo-induced shape memory effect under cyclic compression, respectively.

Dong et al. [41] developed a continuous fiber reinforced honeycomb with repeatable energy absorption based on the cold-programming-induced shape memory effect. These works have demonstrated that material composition, shape memory effects, and unit-cell geometry strongly influence recovery behavior. However, most existing studies primarily focus on high shape recoverability or reporting cyclic responses for specific material-configuration combinations, while the competition between energy-absorbing capacity and shape recoverability remains insufficiently understood.

In this study, three types of meta-honeycomb structures, hexagonal (HEX), auxetic re-entrant (ARE), and double arrow-head (DAH), were fabricated using 3D printing with Nylon and chopped carbon-fiber-reinforced nylon (Onyx). Quasi-static cyclic compression tests were conducted under both in-plane and out-of-plane loading directions, with controlled cycling at different deformation stages. Key performance metrics, including specific energy absorption (SEA), undulation of load-carrying capacity (ULC), shape recovery ratio (SRR), and energy dissipation ratio (EDR), were systematically evaluated. Finite element models were further developed and validated against experimental results to elucidate deformation mechanisms and configuration-dependent responses.

The primary contribution of this work lies in revealing a fundamental trade-off between energy absorption and shape recoverability under cyclic compression. By systematically correlating material selection, topology, loading direction and cyclic deformation stage with both crashworthiness and recovery performance, this study reveals the universality of the trade-off between energy absorption and shape recovery. Moreover, a clear stage-dependent degradation of energy-absorbing capacity under cyclic loading is identified, together with a pronounced sensitivity to loading direction. Finally, a set of quantitative metrics is introduced to characterize repeatable energy absorption and shape recovery, providing new insights and practical guidelines for the design of reusable energy-absorbing architected honeycombs.

2. Materials and methods

2.1 Specimen design and preparation

The honeycomb structures proposed in this paper are divided into three configurations; one non-auxetic Hexagonal (HEX), and two auxetics, namely, Auxetic Re-Entrant (ARE) and Double Arrow-Head (DAH) honeycombs. For these honeycombs, the specific geometric parameters and the topologies of different unit cells are shown in Figs. 1 (a)-(c).

There are three key geometric parameters corresponding to the three honeycomb configuration designs, which are the length (l_h, l_a and l_d), width (w_h, w_a and w_d) and wall thickness (t_h, t_a and t_d) of a honeycomb unit cell. For the HEX and ARE unit cells, the geometry is characterized by a single defining angle, denoted as θ_1. In contrast, the DAH configuration involves two independent geometric parameters, including the main cell angle θ_1 and an additional arrow angle θ_2. To

facilitate the comparison of crashworthiness of different configurations, the relative densities of HEX, ARE and DAH are guaranteed to be consistent, which are defined as the ratio of the material volume of the structure to its occupied volume. The relationship between their relative density and geometric parameters is given as follows:

$$\bar{\rho}_{\mathrm{HEX}} = \frac{2(l_h + w_h \sin(\theta_1/2) - l_h \cos(\theta_1/2))t_h}{(2w_h \sin(\theta_1/2) - l_h \cos(\theta_1/2))l_h} \tag{1}$$

$$\bar{\rho}_{\mathrm{ARE}} = \frac{(w_a \sin(\theta_1/2) + l_a)t_a}{(w_a \sin(\theta_1/2) - l \cos(\theta_1/2))l_a} \tag{2}$$

$$\bar{\rho}_{\mathrm{DAH}} = \frac{(4w_d \sin(\theta_1/2) + 2l_d \cos(\theta_2/2))t_d}{(2w_d \sin(\theta_1/2)\cos(\theta_2/2) - l_d \cos(\theta_1/2)\cos(\theta_2/2))l_d} \tag{3}$$

where $\bar{\rho}_{\mathrm{HEX}}$, $\bar{\rho}_{\mathrm{ARE}}$, $\bar{\rho}_{\mathrm{DAH}}$ are the relative densities of HEX, ARE and DAH.

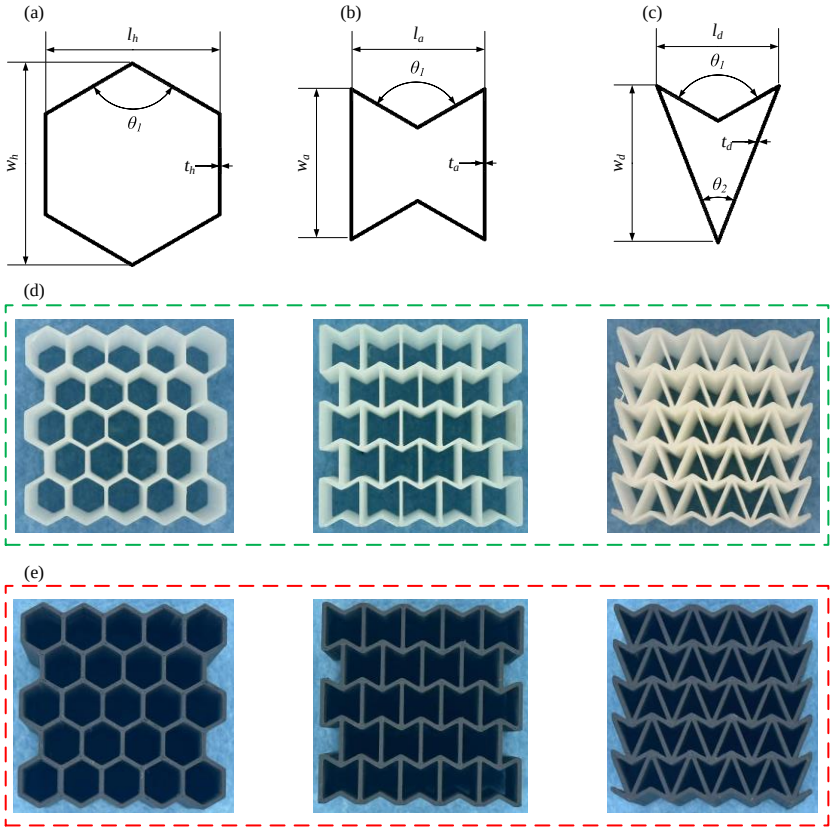


Fig. 1. Design and preparation of honeycombs. Unit cell topologies of: (a) HEX, (b) ARE and (c) DAH. (d)-(e) 3D printed specimens manufactured with Nylon (white material) and Onyx (black material).

Specimens were printed using a Markforged MarkTwo 3D printer (Markforged Holding Co., USA) by fused filament fabrication. All specimens were sliced into 250 layers of the same height during printing, with a height of 0.2 mm for each layer, and printed in the same orientation to ensure the same mechanical properties. Two different materials, Nylon and

chopped carbon fiber reinforced nylon (Onyx), were used for printing. Onyx is made by blending chopped carbon fiber into Nylon, of which the fiber volume fraction is 15 % [42]. The six different specimens prepared by 3D printing are shown in Figs. 1 (d) and (e). As we can see, typical honeycombs specimens (HEX, ARE and DAH) are composed of 5 × 5 unit cells and have the same occupied volume of 50 × 50 × 50 mm^3. The dimensions of the specimens are sufficient to avoid out-of-plane deformation during the test. Three identical specimens were printed for each cyclic compression test and stored at room temperature for five days before testing to achieve full curing.

2.2 Material characterization

Nylon and Onyx, as materials for energy absorbers, exhibit shape recovery characteristics of viscoelasticity and elasto-viscoplasticity properties. In order to obtain the material properties required for numerical simulation, uniaxial tensile tests (ASTM D638-14) and uniaxial compressive tests (ASTM D695-15) were conducted using a universal testing machine (Zwick Z100) to characterize their elasto-plastic properties, and their dynamic mechanical properties were characterized using a dynamic mechanical analyzer (Netzsch 242E) with beam-like specimens (30 × 3 × 2 mm). Dynamic mechanical analysis (DMA) tests were conducted in Isothermal temperature/Frequency Sweep mode, with an amplitude of 0.09 mm and a frequency range from 0.1 to 100 Hz at room temperature. Twenty different frequencies were tested to ensure the smoothness of curves. During the material characterization process, three specimens were tested for each material/structure. The mean curves and error band of mechanical properties are provided in Fig. 2. The Prony series for viscoelasticity of Nylon and Onyx were calculated from DMA data, using the method in Ref. [43] and are given in Table 1.

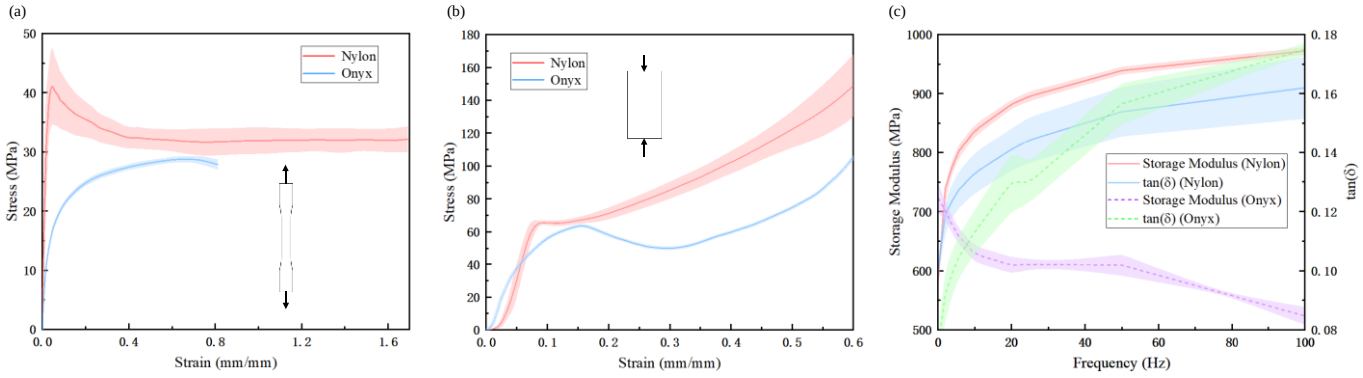


Fig. 2. The stress-strain curves in: (a) the tensile test and (b) the compressive test and (c) DMA curves of Nylon and Onyx.

Table 1. Prony series for viscoelasticity of Nylon and Onyx.

Material	i	g_i	k_i	τ_i
Nylon	1	0.1845	0	0.0545
	2	0.1817	0	1.2084
Onyx	1	0.1905	0	0.0448
	2	0.1141	0	1.1323

2.3 Compressive tests and relative criteria

Quasi-static cyclic compressive tests on the 3D printed honeycomb specimens were performed by a universal testing machine (Instron 4045). The crosshead moving rates of 10 mm/min and 5 mm/min [29] were applied to the loading and unloading processes, respectively. During unloading, after the crosshead detached from the specimens, it continued to return to its initial position at the prescribed unloading rate. In this return-to-zero stage, the specimens were under zero-load conditions and free of displacement constraints, allowing free viscoelastic shape recovery. For a given applied compressive strain, this recovery process provided the same available recovery time in each cycle. To further eliminate the influence of different compressive strain levels on the recovery history, an additional 1 min zero-load dwell period was applied after the unloading process was completed [44]. The recovered height was measured at the end of this dwell period. The load-displacement data were recorded to evaluate the crashworthiness of honeycombs. The specimens were subjected to in-plane cyclic compressive loading in the transverse and longitudinal directions. The in-plane directions, including transverse and longitudinal directions, and out-of-plane direction of the specimens are illustrated in Fig. 3. In the loading-unloading cyclic compressive test, each specimen was compressed to its densification strain (0.6-0.7, which depends on its configuration) as the target strain endpoint. All tests were performed at room temperature of 23 °C, and each specimen experienced three complete loading-unloading cycles and one final compression, and each testing condition was independently repeated three times using different specimens.

During energy absorption, structures usually undergo three stages, namely the linear elastic, the plateau and the densification stages. The first local maximum force observed in the curves is called the initial peak load, which is equivalent to the acceleration level of the protected object when it is impacted, and simultaneously marks the onset of the plateau stage. In general, a lower initial peak load can better protect the object from initial damage. The onset of the densification stage is determined based on the energy absorption efficiency (EAE), where the densification strain is defined as the strain corresponding to the global maximum of the EAE curve [45]. This point marks the transition from the plateau stage to the

densification stage and is applied consistently to all configurations, materials and loading directions. The expression of EAE is given as:

$$EAE = \frac{\int_0^{\varepsilon_c} \sigma(\varepsilon)\mathrm{d}\varepsilon}{\sigma(\varepsilon)} \tag{4}$$

where ε and ε_c are the compressive strain and total compressive strain respectively, and $\sigma(\varepsilon)$ is the compressive stress.

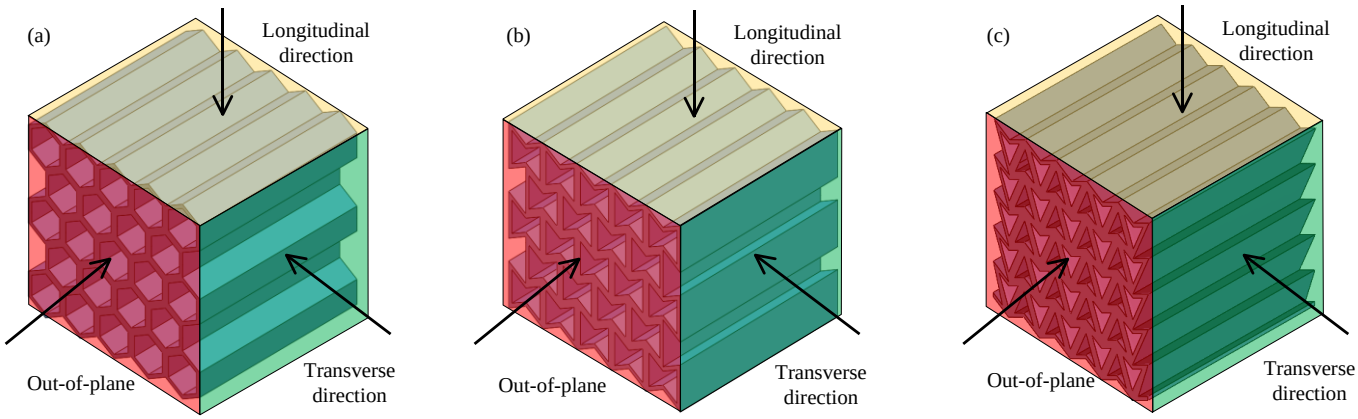


Fig. 3. Transverse, longitudinal and out-of-plane directions of: (a) HEX, (b) ARE and (c) DAH structures.

To evaluate the energy absorption characteristics and shape recovery performance of structures in crashes, some criteria are used to quantitatively describe these behaviors. These criteria include energy absorption (EA), specific energy absorption (SEA), undulation of load-carrying capacity (ULC) [46, 47], shape recovery ratio (SRR) and energy dissipation ratio (EDR) [48].

EA represents the total energy absorbed by a structure during the energy absorption, which can be expressed as:

$$EA = \int_0^l F(x)\mathrm{d}x \tag{5}$$

where $F(x)$ is the compressive load, x and l are the compressive displacement and total compressive displacement, respectively. EA reflects the overall energy absorption capacity of a structure, but SEA is a more critical measure of crashworthiness, which is defined as the energy absorbed by a structure per unit mass as follows:

$$SEA = \frac{EA}{m} \tag{6}$$

where m denotes the mass of each respective structure.

ULC refers to the fluctuation of the stress level during the energy absorption process. A structure with a lower ULC exhibits a more stable stress-strain response, indicating smoother load transfer, which generally corresponds to better energy absorption efficiency and load-bearing stability [44]. The expression of ULC is given as:

$$ULC = \frac{\int_0^{\varepsilon_c} \left|\sigma(\varepsilon) - \sigma_{\text{avg}}\right| \mathrm{d}\varepsilon}{\int_0^{\varepsilon_c} \sigma(\varepsilon) \mathrm{d}\varepsilon} \tag{7}$$

where the average stress σ_{avg} represents the mean stress in the whole compression process, which has the following expression:

$$\sigma_{\text{avg}} = \frac{1}{\varepsilon_c} \int_0^{\varepsilon_c} \sigma(\varepsilon) \mathrm{d}\varepsilon \tag{8}$$

Increasing SEA and decreasing ULC will significantly improve the crashworthiness of the structure. In addition, the discussion on the shape recovery performance criteria is meaningful. SRR represents the ratio of the distance recovered from a structure after being compressed to a certain distance and can be computed as:

$$SRR = \frac{h_r - h_c}{h - h_c} \times 100\% \tag{9}$$

where h, h_c, h_r are the original height of the structures, the height after the structures are completely compressed and the height when the structures are recovered to the limit.

In addition to the analysis of shape recoverability from the perspective of deformation, the structure can also be analyzed from the perspective of energy. Energy release (ER) denotes the energy released during the whole process when a structure undergoes unloading, which depends more on the viscoelasticity of the material. The area enclosed by the loading curve and the unloading curve is the energy dissipation (ED). For each cycle, the integration bounds are defined from the start of loading to the end of unloading. If the unloading curve does not return exactly to the original reference point due to residual deformation, the loop is closed by directly connecting the unloading endpoint to the loading start point [49]. When ED is zero, the structure is unloaded completely according to the loading path, and the structure has a theoretical optimal shape recoverability. EDR is defined as the ratio of ED to EA. The smaller the value of EDR, then the better is the shape recoverability. The related expressions are defined as:

$$ED = \int_0^l F(x) \mathrm{d}x - \int_0^l F_u(x) \mathrm{d}x \tag{10}$$

$$EDR = \frac{ED}{EA} \times 100\% \tag{11}$$

where $F_u(x)$ is the unloading load.

2.4 FE modeling

The FE models of honeycombs under quasi-static compression were developed using the commercial code Abaqus 2021. Specimens were set between two rigid platens to simulate the experimental setup as well as the boundary conditions.

The general contact between the rigid platens and the specimens was defined as hard contact in the normal direction with a tangential friction coefficient of 0.2, while self-contact within the honeycomb structures was enabled using hard normal contact and a lower tangential friction coefficient of 0.1 to account for inter-cell interactions during large deformation and buckling [50]. Dynamic explicit analysis was employed to solve the large-deformation problems using 8-noded element with reduced integration (C3D8R). Quasi-static conditions were achieved by applying a sufficiently low loading rate, and no mass scaling was employed. The ratio of kinetic energy to internal energy remained below 1.5% throughout the simulations, confirming that inertial effects were negligible. To improve numerical stability under severe deformation, distortion control was activated with a length ratio limit of 0.1. In addition, a mesh sensitivity analysis for Nylon specimens was conducted to ensure both computational accuracy and efficiency. Element sizes of 0.4, 0.5, 1.0 and 1.5 mm were examined. The results show that meshes with sizes of 0.4 mm and 0.5 mm yield nearly identical stress-strain responses, while coarser meshes lead to noticeable numerical fluctuations. Considering both accuracy and computational cost, a mesh size of 0.5 mm was ultimately selected for all simulations.

The elastic and plastic behaviors of Nylon and Onyx were modeled by using an elasticity model and a linear Drucker-Prager plasticity model [51], respectively, of which the parameters are obtained from the tests in Section 2.2 and listed in Table 2. The Drucker-Prager model is appropriate here because Onyx exhibits a matrix-dominated response under quasi-static compression, where yielding and irreversible deformation are governed primarily by the pressure-dependent plasticity of the polymer matrix [52]. It should be noted that this model does not explicitly account for fiber fracture, fiber-orientation-dependent tensile reinforcement, or local micro-scale damage accumulation. After the compression simulation, the shape recovery processes of the honeycombs were simulated using restart analysis. All contact, mesh, and other settings were kept consistent with those described above. The viscoelasticity of materials was defined by the Prony series (see Table 1).

Table 2. The elastic and plastic material parameters for Nylon and Onyx.

Material	Young's Modulus (MPa)	Poisson's ratio	Density (g/cm^3)	Angle of friction (°)	Flow stress ratio	Dilation angle (°)
Nylon	826	0.43	1.10	12	0.78	12
Onyx	1392	0.38	1.20	12	0.88	12

3. Results and discussions

3.1 Experimental and numerical investigation of mechanical responses

3.1.1 Finite element model validation

According to the test standard, as described in Section 2, in-plane (transverse and longitudinal direction) cyclic compression tests were performed on the specimens and FE simulations were performed of their first cyclic compression. The mechanical responses and deformation modes obtained by the two methods were compared to verify the effectiveness of the FE simulation. Then, relevant parameters, such as SRR, EDR, SEA, ULC and related parameters were calculated and compared for the honeycombs with different materials and configurations to further analyze the performance differences.

The longitudinal compression and recovery processes of HEX, ARE and DAH are illustrated in Fig. 4 with experimental data above and FE simulation below. The strain levels of 0, 0.2, 0.6, and 0.7 correspond to different compression stages, whilst strain levels of 0.5, 0.3, and 0.1 represent various recovery stages. As shown in Fig. 4(a), deformation in the HEX structure initiates in the central band and subsequently propagates to the adjacent two rows of cells. Eventually, the deformation extends to the lateral sides, leading to an overall densification of the structure. As can be seen in Fig. 4(b), ARE structure exhibits non-typical auxetic behavior under longitudinal compression, primarily because the unit cells are prone to local instability and buckling in this direction. During the compression process, the vertical walls of adjacent bands in the ARE structure rotate in opposite directions, resulting in lateral displacement of the bands. This deformation weakens the negative Poisson's ratio characteristic but does not eliminate it, and the residual auxetic effect still contributes to the shape recovery process. Similar to HEX, failure in ARE initiates in the central band and progressively spreads toward the sides. As can be seen in Fig. 4(c), the side walls of DAH undergo varying degrees of buckling during compression. Due to the different buckling behaviors among unit cells, the bands of DAH collapse and tilt in different directions. Specifically, the second band exhibits an inward concavity, while the fourth band shows an outward convexity, resulting in an overall S-shaped deformation mode. This causes some unit cells to rotate during compression, and the initially arrow-shaped voids gradually evolve into rectangular shapes. During unloading, all three structures exhibit a global shape recovery, with all five bands being unfolded simultaneously and gradually returning toward their original configuration. However, due to energy dissipation during the deformation process, full recovery is not achieved. All three structures recover to 50-80 % of their original height, depending on their configurations and material properties. Fig. 4 also compares the deformation processes obtained from experiments and simulations, indicating that the finite element results

accurately capture the structural deformation during both the compression and recovery phases.

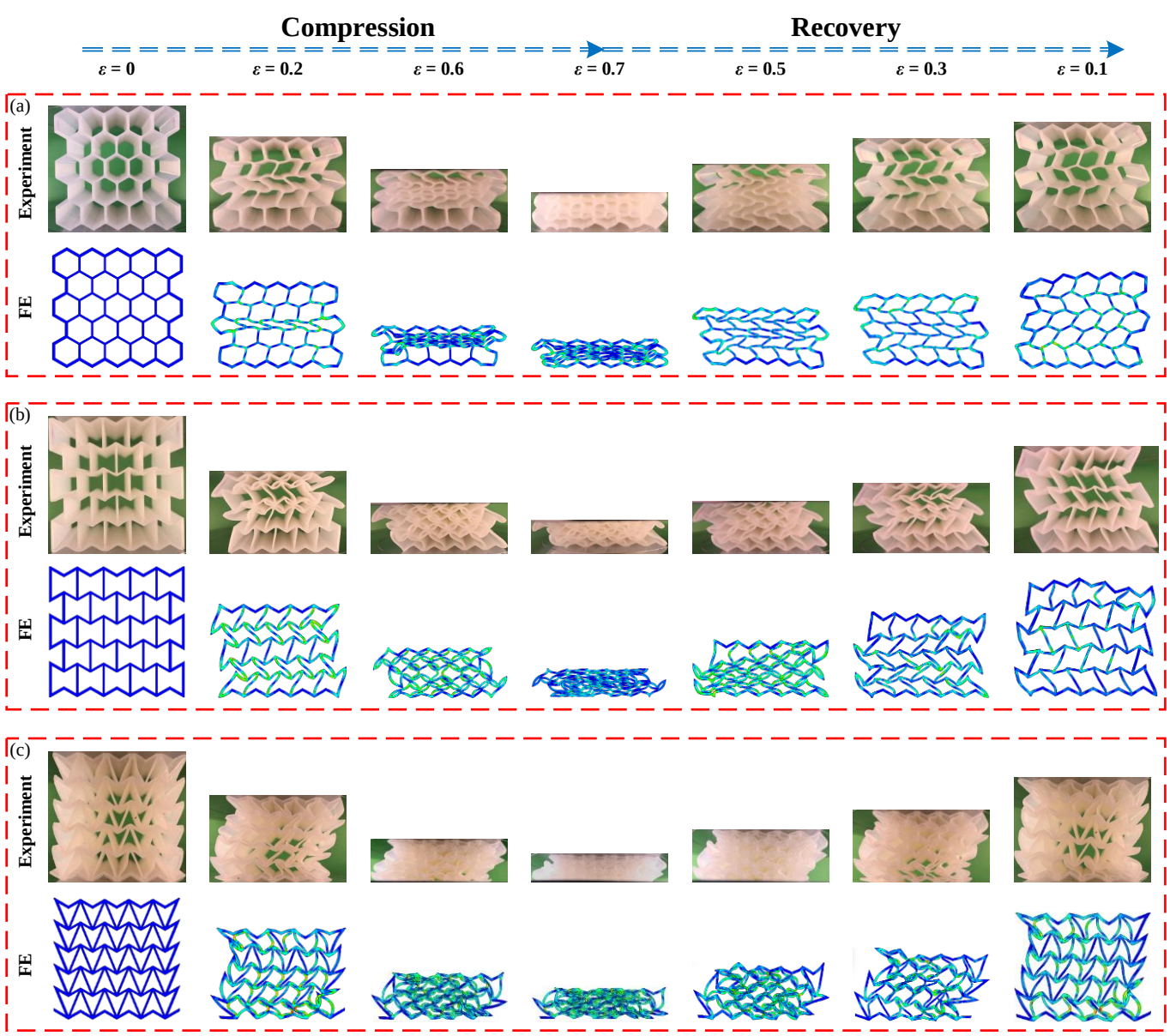


Fig. 4. Deformation processes of: (a) HEX, (b) ARE, and (c) DAH under longitudinal compression and recovery.

3.1.2 Observed mechanical responses and deformation modes

Fig. 5 presents the stress-strain curves of HEX, ARE, and DAH fabricated from Nylon and Onyx under multiple cycles of compression in the longitudinal direction, along with the finite element results of the first cycle. From Fig. 5, it can be observed that all three honeycombs reach their initial peak stress for strains less than or slightly greater than 0.1, followed by an extended plateau stage, and finally enter a densification phase characterized by a sharp stress increase. The densification strains are quantitatively determined from the global maximum of the EAE, with values of 0.64, 0.55, and 0.52 for Nylon HEX, ARE, and DAH, respectively, and 0.58, 0.53, and 0.51 for Onyx HEX, ARE, and DAH, respectively.

For the Nylon specimens, the initial peak and plateau stresses are approximately at the same level across all three honeycomb structures, with a notable stress rise only in the densification stage. In contrast, the Onyx specimens show a significantly higher initial peak stress, about 1.5 times the plateau stress. The plateau stresses range from 0.1-0.8 MPa for Nylon and 0.6-3.8 MPa for Onyx. Specifically, the Onyx HEX, ARE and DAH structures exhibit 222, 369 and 411 % increases in plateau stress, respectively, compared to their Nylon counterparts. The influence of structural configuration on energy-absorbing capacity is further discussed in Section 4.2. Additionally, from the second and third cycles, the initial peak stress disappears, giving way to a smoother rising curve across all configurations, indicating material softening or structural adaptation. In summary, Onyx significantly enhances both the initial peak and the plateau stress, thereby improving the energy-absorbing capacity of the honeycomb structures. It should be noted that the chopped fiber reinforcement in Onyx is assumed to provide a relatively homogeneous enhancement of stiffness and strength. For further studies, controlling the orientation of continuous fibers may lead to different deformation modes and altered recovery behavior under cyclic compression [53].

In addition to longitudinal cyclic compression, the stress-strain responses of the honeycomb structures under transverse cyclic loading were also recorded, as shown in Fig. A.1, Appendix. The trend of curves is similar to those observed under longitudinal loading. However, the transverse stress-strain curves appear smoother, which is likely attributed to the increased contact area between the structure and the compression platens in the transverse direction. This enhanced contact area improves structural stability during crushing.

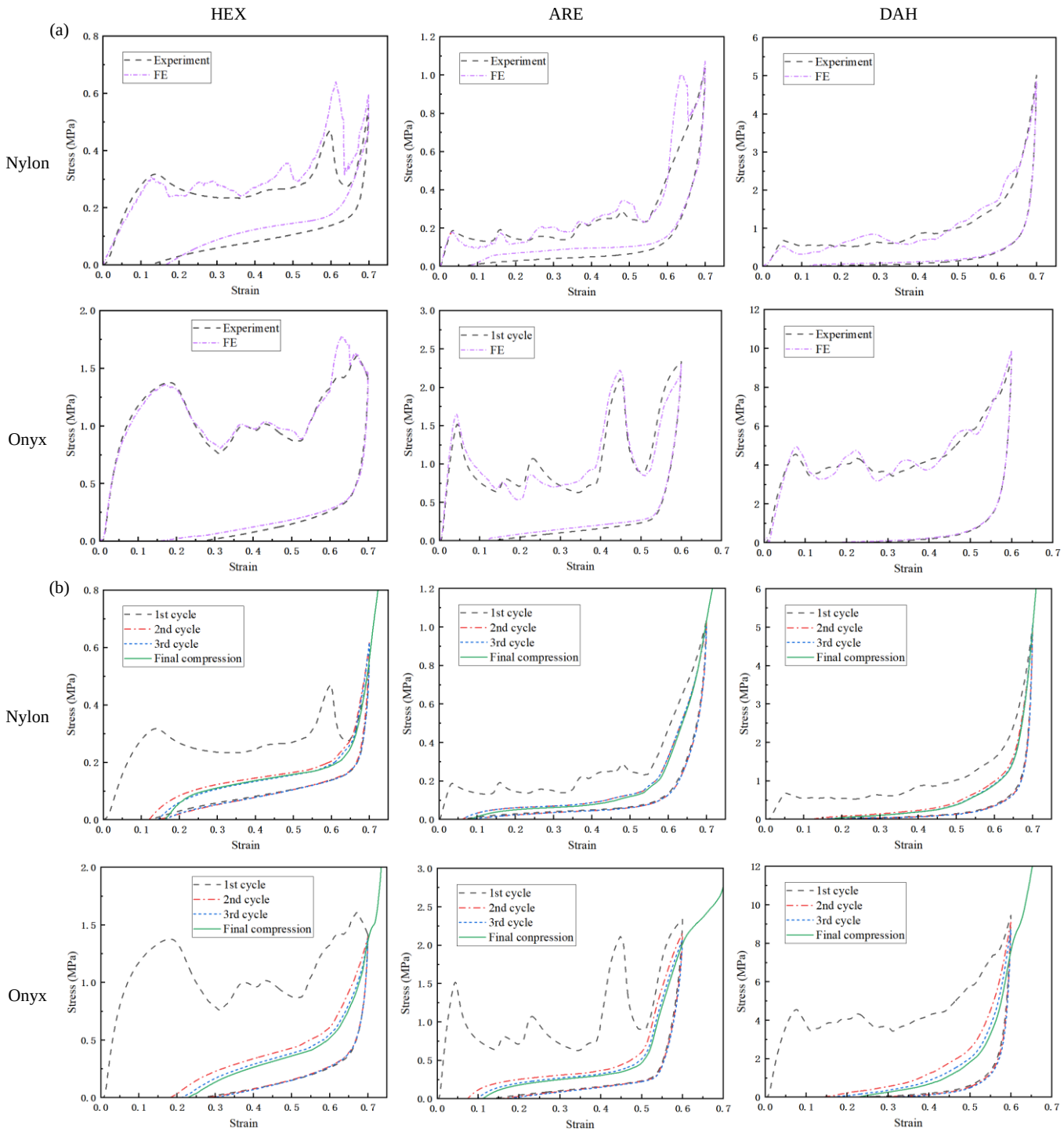


Fig. 5. The stress-strain curves of honeycomb structures (HEX, ARE and DAH): (a) experimental and FE results for the first compression cycle and (b) cyclic compressions in the longitudinal direction.

3.2 Repeatable energy absorption under cyclic loading

To evaluate the crashworthiness of honeycombs with different materials and configurations during multiple cycles of compression, SEA and ULC were calculated according to the stress-strain curves, as plotted in Fig. 6. Figs. 6 (a)-(c) show the SEA values of various honeycombs under longitudinal cyclic loadings. It can be seen from Figs. 6 (a)-(c) that no matter

what kind of material or configuration of honeycombs, their SEA values decrease with the increase of the number of cycles. This trend can be well explained because as the number of cycles increases, the stiffness of honeycombs after compression is degraded and the fracture damages are aggravated. It is also shown in Figs. 6 (a)-(c) that the performance degradation of the honeycombs after initial compression is the most severe. In the subsequent compressions, the structural damage of the honeycombs due to the compression at the same strain is much less than that of the initial compression. In addition, we can see that the SEA of Onyx honeycombs are much higher than that of Nylon ones under the same cycle. Compared with Nylon, Onyx enhances the stiffness and strength of the matrix due to the mixing of chopped carbon fiber. This is an excellent improvement for the crashworthiness of the structures.

In addition to structural damage accumulation, the degradation of SEA with increasing cycle number is closely associated with pronounced stress-softening behavior under cyclic compression. After the first cycle, all honeycomb configurations exhibit a noticeable reduction in stiffness and peak stress in subsequent cycles, as shown in Fig.5, which is characteristic of Mullins effect in polymer-based structures [54]. It is most significant between the first and second cycles, corresponding to the initial establishment of stable deformation modes and preferential collapse paths. Once these deformation paths are formed, subsequent loading tends to follow the pre-conditioned bending and buckling configurations, leading to a relatively stabilized mechanical response and a slower rate of SEA degradation [55]. This mechanism provides a rational explanation for the sharp reduction of SEA after the initial compression and its more gradual evolution in later cycles.

Figs. 6 (d)-(f) compare the ULC values of the honeycombs with different materials and configurations, indicating the trend of ULC with the number of cycles. It can be seen from the figures that the honeycombs made of different materials show lower ULC values during the initial compression process, which indicates that the energy absorption of the structures is relatively stable and the energy absorption efficiency is higher. However, in the second and third cycles, ULC values of the Nylon and Onyx honeycombs increase significantly, indicating that the energy absorption process of the structures is no longer stable after the initial compression damage and shape recovery. As illustrated by the stress-strain curves in Fig. 5, the honeycomb structure exhibits a distinct initial peak stress and plateau stage during the first compression cycle. With increasing strain, progressive structural damage occurs, resulting in a relatively smooth transition from the plateau stage to the densification one. However, after multiple compressions, the structural integrity deteriorates significantly due to accumulated local buckling and damage. This leads to a reduction in overall stiffness, causing the reduction of the initial peak and plateau stresses, which further widens the stress level gap between the plateau and densification stages with a

higher ULC being produced. It is worth noting that during the first cycle of compression, slight fluctuations in stress already appear within the plateau stage, which can influence the ULC to some extent. However, such fluctuation is not a dominant factor. The ULC is primarily governed by the difference between the maximum and minimum stress levels throughout the loading path, particularly between the plateau and densification stages. Therefore, due to the increased instability in the load-bearing response of the honeycomb structure, it exhibits a greater ULC after multiple compression cycles compared to the first cycle.

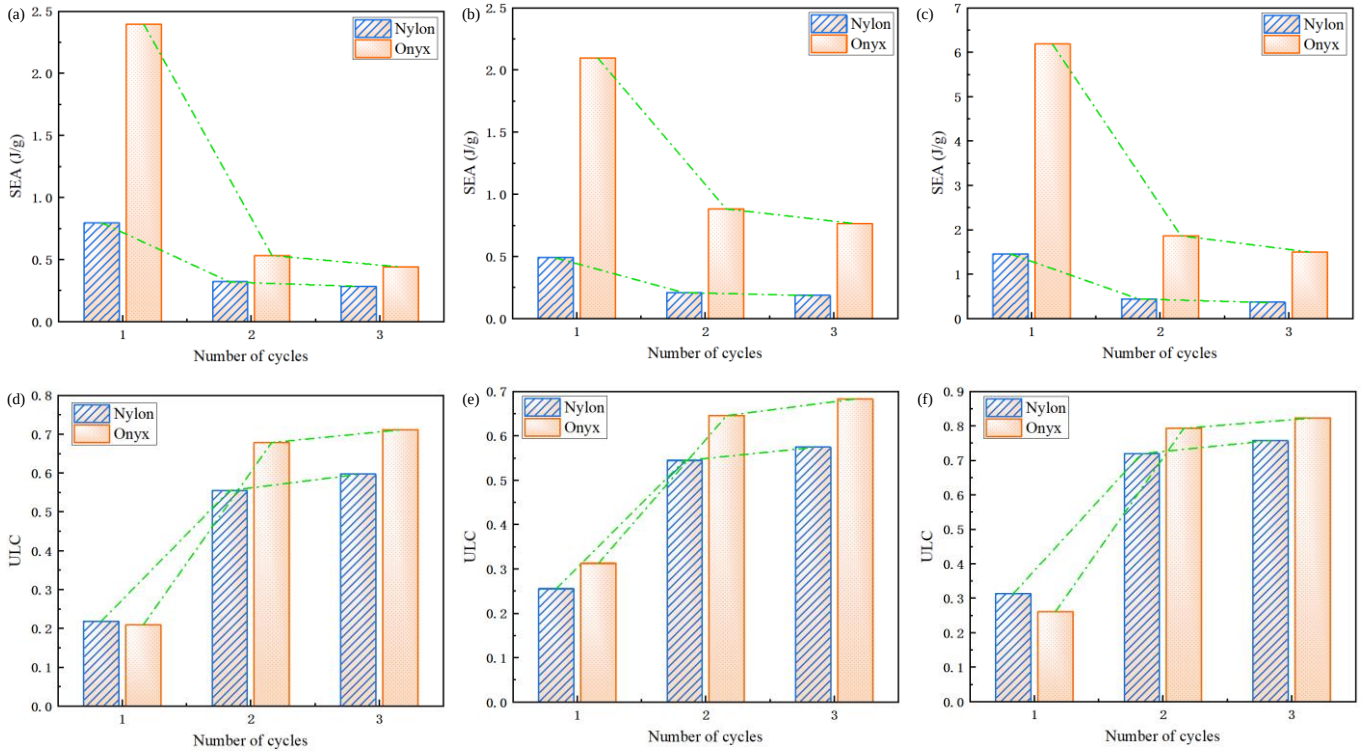


Fig. 6. Specific Energy Absorption (SEA) of: (a) HEX, (b) ARE, (c) DAH and Undulation of Load-Carrying capacity (ULC) of: (d) HEX, (e) ARE, (f) DAH under longitudinal cyclic loading.

3.3 Shape recoverability of honeycombs

In the cyclic compression tests, it is found that the honeycomb specimens have shape recovery characteristics. To further explore the influence of different configurations and materials on this characteristic, SRR and EDR of the honeycomb specimens subjected to transverse and longitudinal cyclic compressions are calculated. Figs. 7(a)-(c) show the comparisons of SRR of honeycombs under longitudinal cyclic loading. It can be clearly seen that as the number of cycles increases, SRR shows a downward trend. This trend is applied to both Nylon and Onyx specimens with different configurations. By comparing the shape recovery performance of Nylon and Onyx specimens, it can be confirmed that the shape recoverability of Nylon is clearly better. In Section 3.2, it has been found that the energy absorption capacity of Onyx specimens with the same configuration is higher than that of Nylon specimens. Therefore, we can conclude that the

crashworthiness and shape recoverability of a material are a pair of contrary evaluation indicators. It can be considered that if the energy absorption of an energy absorber made of one material is higher than that of another material in the initial crash process, then the number of times that this material can effectively absorb the crash energy will be lower than that of another material. It should be noted that according to the different definitions of the effective value of energy absorption, the effective number of energy absorption will also change.

In addition, a clear dependence of shape recoverability on the effective Poisson's ratio of the honeycomb configuration can be identified by comparing different topologies. For both materials, the auxetic configurations (ARE and DAH) consistently exhibit higher SRR values than the conventional honeycomb (HEX) under the same loading conditions and cycle numbers. This indicates that shape recovery is not governed by material behavior alone but is strongly influenced by topology-induced deformation kinematics. For the honeycomb with a positive Poisson's ratio, axial unloading is accompanied by lateral contraction, and height recovery relies almost exclusively on material elasticity and viscoelastic relaxation. Once plastic bending, micro-buckling, or irreversible hinge formation occurs, the axial recovery becomes highly sensitive to accumulated damage, resulting in a rapid degradation of shape recovery with increasing cycle number. In contrast, auxetic honeycombs with a negative Poisson's ratio exhibit a geometrically assisted recovery mechanism. During unloading, the reverse rotation of re-entrant or arrow-shaped cell walls induces lateral deformation that is kinematically coupled to axial extension. This coupling introduces an additional geometry-driven recovery component in the height direction, which partially compensates for material-level plastic damage [44]. As a result, auxetic structures retain higher SRR compared with positive Poisson's ratio configurations.

The repeatable energy absorption capacity of structures is not only reflected in the shape recovery but also depends on the efficiency of energy release and dissipation during cyclic loading, which is calculated and plotted in Figs. 7(d)-(f). As we can see from the figure, the EDR value of the initial compression is close to 100 %. However, after multiple cyclic compressions, EDR drops to a stable value. It is generally believed that a higher EDR indicates that most of the energy is dissipated through plastic deformation, reflecting strong damping characteristics, whilst a lower EDR suggests that most of the absorbed energy is stored as elastic energy, implying better shape recoverability. However, it can be seen from the stress-strain curves of the shape recovery stage in Fig. 5 that the ER by the same material and configuration of the honeycombs during each unloading process is very close, but the EA value decreases significantly. The decrease in EDR is likely attributed to a significant decrease in EA, which leads to a decrease in stored elastic energy and consequently diminishes the structural shape recovery performance. Therefore, we can conclude that damage to the structure greatly

affects the energy absorption capacity. However, this has little effect on the shape recoverability.

In addition, the SEA, ULC, SRR, and EDR of the honeycombs under in-plane transverse cyclic loading were analyzed (Figs. A.2 and A.3, Appendix). The results show that all indicators exhibit trends consistent with those observed under in-plane longitudinal loading, indicating that the performance trends are largely isotropic within the plane. Importantly, the trade-off between crashworthiness and shape recoverability persists under transverse loading. These findings confirm that the competing relationship between energy absorption and shape recovery is independent of loading direction, further reinforcing the generality of the observed performance trends.

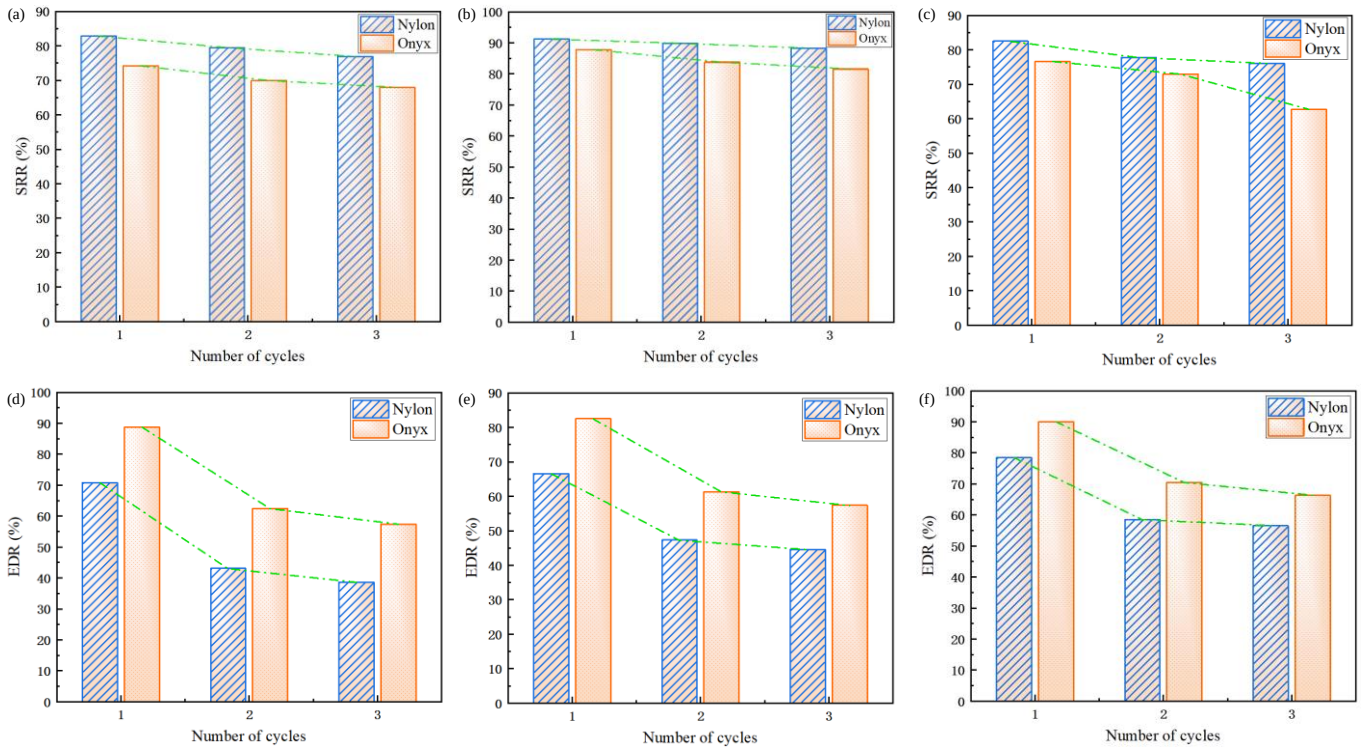


Fig. 7. Shape Recovery Ratio (SRR) of: (a) HEX, (b) ARE, (c) DAH and Energy Dissipation Ratio (EDR) of: (d) HEX, (e) ARE, (f) DAH under longitudinal cyclic loading.

4. Parametric studies of cyclic compression process

4.1 Comparisons between in-plane and out-of-plane cyclic compressions

In general, both the energy-absorbing behavior and the shape recovery performance of the same honeycomb structure show consistent trends under cyclic compression along different in-plane directions. The influence of materials on SEA, ULC, SRR and EDR has been discussed in Section 3, where Nylon and Onyx exhibit similar qualitative trends with different magnitudes. Moreover, extensive literature on Nylon honeycombs has reported the differences between in-plane and out-of-plane responses, which are in agreement with the trends observed in this study for Onyx specimens [56]. Therefore, only Onyx specimens are selected to carry out the out-of-plane cyclic compression tests, and the stress-strain

curves are shown in Fig. 8.

In order to further explore the influence of loading in different planes on the crashworthiness of honeycombs, we compare the SEA and SRR obtained by in-plane transverse and out-of-plane cyclic compression tests in Figs. 9 and 10. During the first cycle of compression, the honeycombs with loading applied out-of-plane have better SEA than those with in-plane energy absorption, which shows that the out-of-plane direction of honeycombs is most suitable for energy absorption, and this direction has the best crashworthiness. According to the EAE method described in Section 2.3, the densification strains are 0.56 for HEX, 0.57 for ARE, and 0.54 for DAH, indicating that all three configurations enter densification at comparable strain levels in this loading mode. After multiple energy absorption, the SEA values of honeycombs with the same configuration decrease significantly and move close with each other regardless of the loading direction. This trend is consistent with those shown in Figs. 6(a)-(c), which proves that honeycombs are most seriously damaged with the most severe degradation of overall stiffness when it undergoes the first compression. By comparing the in-plane and out-of-plane cyclically compressed honeycombs, it can be found that the SRR of honeycombs under in-plane cyclic compression is higher. The maximum differences between the in-plane and out-of-plane SRR of the honeycomb with same configuration is also marked in Fig. 10. The maximum SRR differences between these two loading directions on HEX, ARE and DAH are 26, 35 and 35 %, respectively. The values indicate that the shape recoverability of the in-plane cyclic energy-absorbing honeycombs is improved by 1/4 to 1/3 compared to the out-of-plane ones. Based on the analysis of SEA and SRR, it is further proved that there is a competitive relationship between them for the same material.

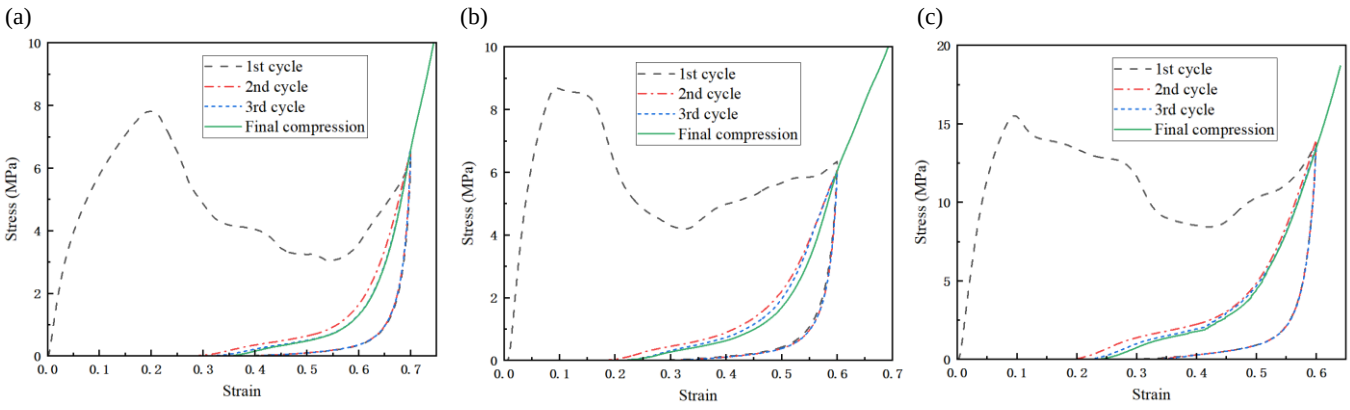


Fig. 8. The stress-strain curves of: (a) HEX, (b) ARE and (c) DAH under out-of-plane cyclic compression.

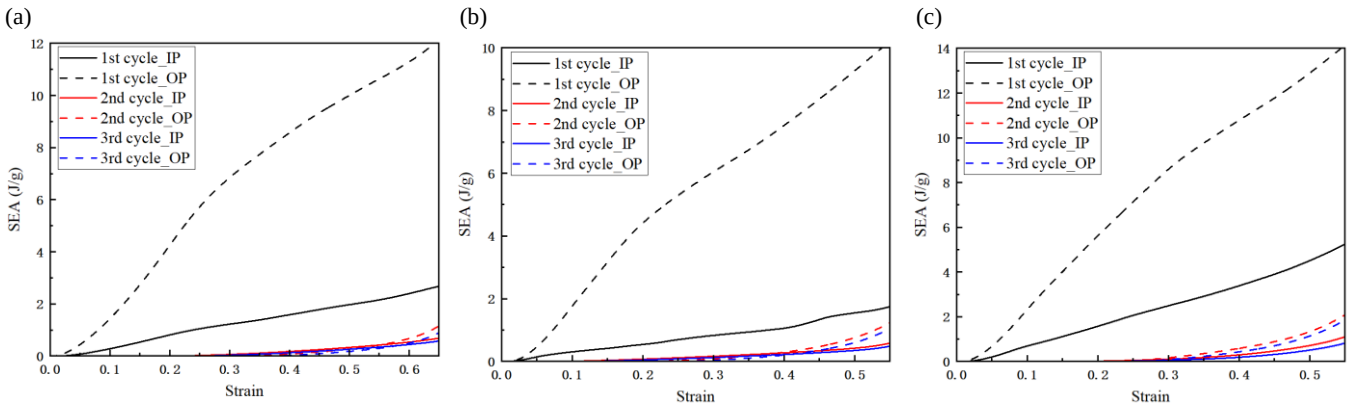


Fig. 9. Comparison of Specific Energy Absorption (SEA) of: (a) HEX, (b) ARE and (c) DAH under in-plane (IP) and out-of-plane (OP) cyclic compressions.

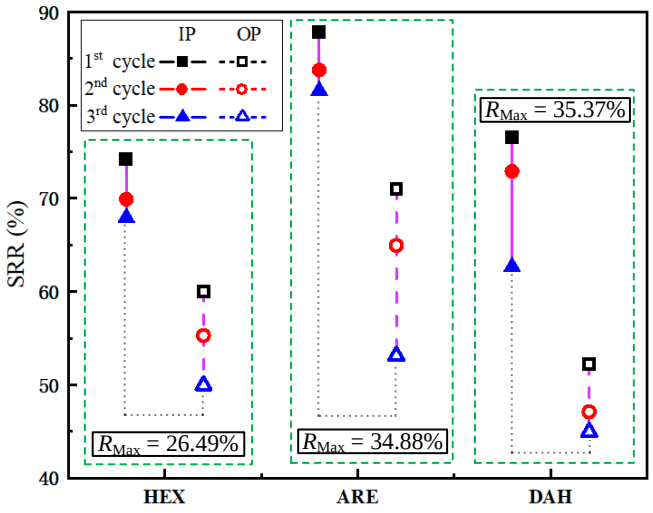


Fig. 10. Comparison of Shape Recovery Ratio (SRR) of HEX, ARE and DAH under in-plane (IP) and out-of-plane (OP) cyclic compressions.

4.2 Effect of structural configuration

In this section, the effect of structural configuration on the energy absorption behavior of honeycombs is analyzed under monotonic transverse compression. The following analysis focuses on the deformation modes, plastic hinge formation and plastic collapse mechanisms that govern the plateau stress. This is without considering cyclic loading or viscoelastic recovery effects.

During energy absorption, when the stress in the honeycomb structure is greater than the critical one, the cell walls will enter a plastic collapse stage. As a result, the plastic hinges will be formed at the node, which corresponds to the plateau stage in the stress-strain curve. In this section, the transverse stress states of honeycombs with three different geometric configurations of HEX, ARE and DAH are analyzed, as shown in Fig. 11.

When HEX and ARE honeycombs are subjected to transverse loading, their stress states are similar because their representative plastic hinges are composed of a horizontal beam joined with a pair of beams diagonally extended to the left or right, respectively. When the honeycombs are under large deformations, the horizontal beam basically maintains the original horizontal state, and the two inclined beams will bend, resulting in plastic collapse and eventually being flattened. When DAH is subjected to transverse loading, the representative plastic hinge will rotate and continue until a peak force is reached. Due to the lack of horizontal beam support, the cell wall of the structure will buckle and fold during large deformation and eventually become flat.

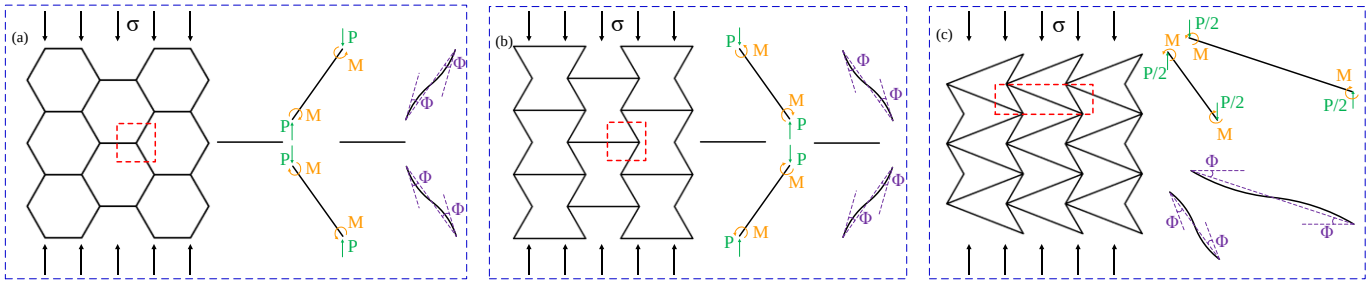


Fig. 11. Schematic diagram of large strain plastic collapse of: (a) HEX, (b) ARE and (c) DAH under transverse quasi-static compression.

The theoretical values of their plastic collapse stresses are given by Eqs. (12)-(14) [12, 14, 57]:

$$\sigma_{\mathrm{pl}} = \frac{\sigma_{ys} t_h^{\,2} \tan(\theta_1/2)}{l_h[w_h \tan(\theta_1/2) - l_h/2]} \tag{12}$$

$$\sigma_{\mathrm{pl}} = \frac{\sigma_{ys}\theta_1[t_a \sin(\theta_1/2)/l_a]^2}{[2w_a \sin(\theta_1/2)/l_a - \cos(\theta_1/2)][\sin(\theta_1/2) - 4t_a \sin(\theta_1/2)/l_a]} \tag{13}$$

$$\sigma_{\mathrm{pl}} = \frac{2\sigma_{ys} \sin(\theta_1/2)\cos(\theta_2/2) t_d^{\,2}}{\sin(\theta_1/2 - \theta_2/2)/l_d^{\,2}} \tag{14}$$

where σ_{pl} is plastic collapse stress and σ_{ys} is yield stress.

Fig.12 shows the comparison between the theoretically calculated plastic collapse stress and the measured plateau stress of Nylon and Onyx honeycombs with HEX, ARE and DAH configurations. It can be observed that the plastic collapse stress is very close to the plateau stress, which indicates that the buckling and plastic collapse of the honeycomb cell walls are the main factors for the formation of the plateau stage. To clarify the differences between the plastic collapse stress and plateau stress, the error analysis of the experimental and theoretical stresses is carried out, and the specific stress values and errors are given in Table 3. The results show that the errors of the stresses are less than 10 %, which further verifies the equivalence of the two types of stresses.

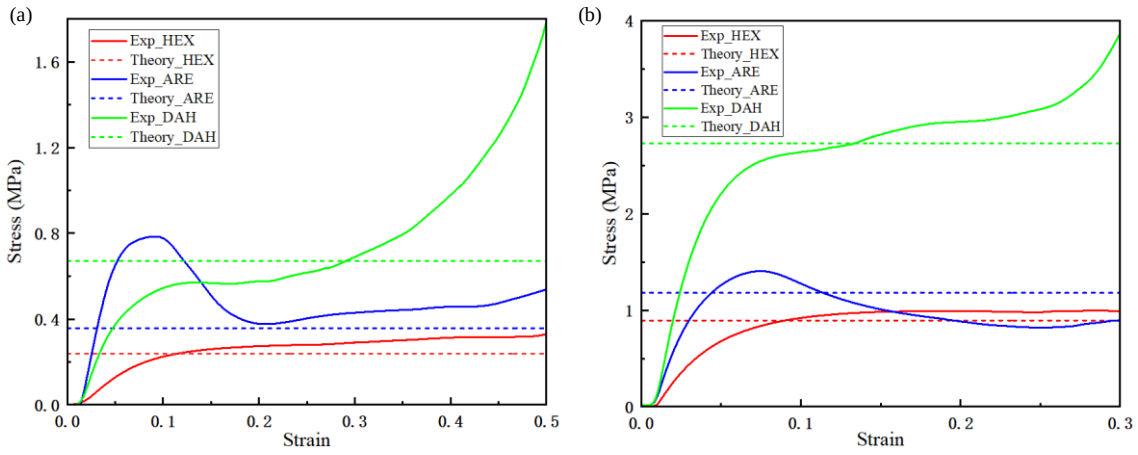


Fig. 12. Experimental and theoretical compressive stress-strain curves of HEX, ARE and DAH made of (a) Nylon and (b) Onyx.

Table 3. Differences between the experimental plateau stress and the theoretical plastic collapse stress.

Specimen ID	Experimental stress (MPa)		Theoretical stress (MPa)		Error (%)	
	Nylon	Onyx	Nylon	Onyx	Nylon	Onyx
HEX	0.2595	0.9887	0.2385	0.9137	8.09	7.59
ARE	0.3782	1.2577	0.3571	1.3681	5.58	8.78
DAH	0.6166	2.8123	0.6697	2.5657	8.61	8.77

4.3 Effect of cyclic strain

As mentioned in Section 2.3, the repeatable energy absorption of honeycombs is divided into three stages, namely the elastic stage, the plateau stage and the densification stage. Therefore, stage-limited cyclic compression experiments were designed, in which repeated loading-unloading was intentionally confined to a specific deformation stage, to clarify how cyclic loading at different deformation stages affects the subsequent crashworthiness of honeycombs. The cyclic compressions conducted within the elastic stage, plateau stage and densification stage are defined as Stage-I cycling, Stage-II cycling and Stage-III cycling (denoted as Cycle I, Cycle II and Cycle III for simplicity), respectively, with three loading-unloading cycles performed at each prescribed stage. For example, Cycle I denotes a test in which the honeycomb undergoes three elastic loading-unloading cycles before a full compression. Fig. 13 shows the stress-strain curves of Onyx honeycombs after stage-limited cyclic compression cycles together with the reference stress-strain curves from the initial monotonic compression without any prior cycling.

As can be seen, the stress-strain curves of compression after Cycle I (elastic-stage cycling) are similar to the curves obtained by the initial compression, indicating that cyclic loading confined to the elastic stage introduces negligible

permanent damage and has little influence on the subsequent crashworthiness and shape recoverability of the honeycombs. In contrast, for the honeycombs compressed after Cycle II (plateau-stage cycling), the stress-strain curves lost the elastic stage and the plateau stage and move into the initial densification stage. This reveals that cyclic loading within the plateau stage induces irreversible deformation and partial loss of load-bearing capacity, although the structures still retain a certain energy absorption capacity at large strains. For the honeycombs compressed after Cycle III (densification-stage cycling), especially for the DAH configuration, the stress-strain curves in the subsequent compression almost completely vanish. This indicates that the cyclic loading in the densification stage leads to severe structural damage and extensive plastic collapse, resulting in a pronounced loss of both crashworthiness and shape recoverability. Consequently, the structure becomes unsuitable for further energy-absorption applications.

The underlying mechanisms responsible for the above phenomena can be attributed to the strain-dependent deformation and energy dissipation behaviors of the honeycomb structures. At low compressive strains corresponding to the elastic stage, deformation is primarily governed by elastic bending and reversible rotation of the cell walls [58, 59]. Only minor micro-buckling may occur, which remains largely reversible. In this regime, energy dissipation is dominated by the viscoelastic hysteresis of the polymer matrix, resulting in limited permanent deformation and high shape recovery. Consequently, cyclic compression within the elastic stage has a negligible influence on the subsequent stress-strain response and crashworthiness of the honeycombs.

As the deformation progresses into the plateau stage, localized micro-buckling intensifies and progressively evolves into irreversible plastic hinge formation at the junctions of the cell walls. In this stage, plastic dissipation gradually becomes dominant over viscoelastic losses, leading to enhanced energy absorption during the initial compression but also inducing cumulative structural damage [60]. As a result, repeated loading-unloading in the plateau stage significantly degrades the recoverability of the honeycomb structure, causing the disappearance of the elastic and plateau regions in subsequent compressions while retaining a certain energy absorption capability at large strains.

When the cyclic compression is further extended into the densification stage, extensive cell wall contact, severe local bending and geometric locking promote widespread plastic collapse and irreversible distortion throughout the structure. Although energy absorption is maximized due to large plastic dissipation, the deformation is no longer governed by recoverable viscoelastic mechanisms. Instead, permanent plastic damage dominates the response, leading to a near-complete loss of structural integrity and crashworthiness in subsequent compressions, as observed for the honeycombs subjected to Cycle III.

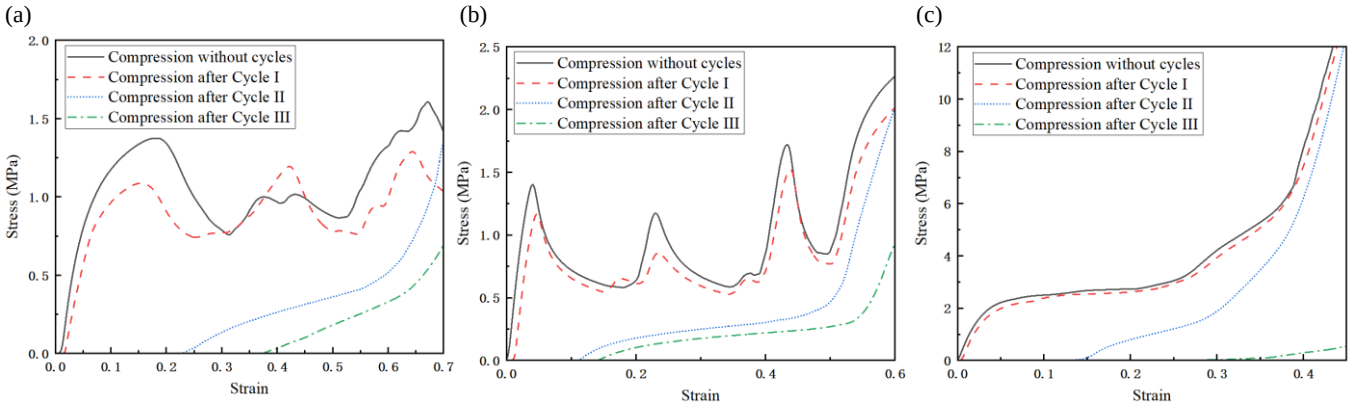


Fig.13. Stress-strain curves of: (a) HEX, (b) ARE and (c) DAH after cyclic compressions at different stages.

To accurately determine the effect of different stages of cyclic compression on the crashworthiness of honeycombs, a non-dimensionless loss ratio of SEA (SEA_r) is proposed in Eq. (15). For the convenience of recording, SEA and SEA_r are also recorded as SEA^{I}, SEA^{II}, SEA^{III} and SEA_r^{I}, SEA_r^{II}, SEA_r^{III} according to the different cyclic compression stages. The definition of SEA_r is as follows:

$$SEA_r^i = \left| \frac{SEA^i - SEA}{SEA} \right| \times 100\% \quad (i = \mathrm{I, II, III}) \tag{15}$$

Table 4 summarizes the SEA and SEA_r values of HEX, ARE and DAH after different stages of cyclic compression. By analyzing SEA_r, it can be seen that the cyclic compressions in the elastic, the plateau and the densification stages reduce SEA values by about 10, 50 and 100 %, respectively.

Table 4. SEA and SEA_r of honeycombs with different configurations after cyclic compression at different stages.

Specimen ID	SEA (J/g)	SEA^{I} (J/g)	$SEAr^{I}$ (%)	SEA^{II} (J/g)	$SEAr^{II}$ (%)	SEA^{III} (J/g)	$SEAr^{III}$ (%)
HEX	3.34	3.01	9.88	1.82	45.51	1.07	67.96
ARE	1.95	1.67	14.36	0.73	62.56	0.12	93.85
DAH	3.65	3.43	6.03	1.63	55.34	0.05	98.63

5. Conclusions, potential applications and future work

5.1 Conclusions

This study has investigated the crashworthiness, deformation modes and energy-absorbing characteristics of three types of honeycomb structures under cyclic compression. In addition, the effects of fiber reinforcement, compression direction, honeycomb configurations, number of cycles and cyclic strain on crashworthiness and shape recoverability have been systematically examined. Based on the findings of this study, the following conclusions can be drawn:

(1). The Specific Energy Absorption (SEA) decreases with increasing cycle numbers. Due to the incorporation of

short carbon fibers, Onyx exhibits significantly higher stiffness and strength compared to Nylon, resulting in a substantially higher SEA. During the initial compression stage, the honeycombs show a low Undulation of Load-Carrying capacity (ULC) and high energy absorption efficiency. However, after repeated compression, the structure lacks sufficient strength to generate an initial peak load and stress fluctuations become less distinct due to stiffness degradation.

(2). The Shape Recovery Ratio (SRR) shows a downward trend with increasing cycle numbers. Nylon demonstrates relatively better shape recovery than Onyx, which indicates a contradiction between crashworthiness and shape recoverability for the same material. If a structure absorbs more energy than another one during the initial compression, its capacity to continue absorbing energy over multiple cycles is likely to be lower. The decline in Energy Dissipation Ratio (EDR) is primarily due to the significant reduction in Energy Absorption (EA), suggesting that structural damage severely compromises the energy absorption capability but has a relatively minor effect on shape recovery.

(3). During the first compression cycle, the out-of-plane SEA of the honeycombs is higher than the in-plane one, indicating superior crashworthiness in the out-of-plane direction. However, the shape recovery capability of honeycombs under in-plane cyclic compression is approximately 25% to 35 % greater than that under out-of-plane loading, further demonstrating the inherent contrary effect between energy absorption and shape recovery for the same material.

(4). Under cyclic compression at different deformation stages, the elastic stage has minimal impact on crashworthiness, while honeycombs compressed in the densification stage almost completely lose their energy absorption capacity. Specifically, cyclic compression in the elastic, plateau, and densification stages reduces SEA by approximately 10, 50, and 100 %, respectively.

The competing relationship between repeatable energy-absorbing characteristics and shape recovery performance, together with the effects of key structural and loading parameters on the energy absorption studied in this paper, provides valuable data for assisting the design of reusable energy absorbers.

5.2 Potential applications

The identified trade-off between crashworthiness and shape recoverability highlights the need for application-specific design strategies. For reusable energy-absorbing components subjected to repeated or low-to-moderate loading, preserving structural integrity and shape recovery is critical. In such cases, excessive plastic dissipation accelerates performance

degradation. As a result, configurations with higher recoverability are preferred, especially auxetic honeycombs with geometrically assisted recovery [44, 61].

In contrast, for single-use or sacrificial structures designed for severe impact events, such as automotive crash boxes, maximizing energy absorption takes precedence over shape recoverability. Conventional honeycombs with positive Poisson's ratio, especially when loaded in the out-of-plane direction, promote stable progressive collapse and high energy dissipation, and are therefore more appropriate. These results indicate that Poisson's ratio, topology and loading direction should be selected according to service requirements, rather than optimized solely for peak energy absorption.

5.3 Future work

While this study systematically reveals the inherent trade-off between energy absorption and shape recoverability, it is still an open challenge to fully resolve it. Hierarchical and multi-level architectures represent a promising strategy to redistribute deformation from localized failure to progressive plastic collapse, potentially improving both crashworthiness and recoverability [51]. However, identifying optimal designs that balance these competing objectives remains a challenging, high-dimensional problem.

Future work will therefore focus on integrating data-driven and machine-learning-assisted design approaches with physics-based modeling to explore the vast design space of architected materials [62]. Such approaches may enable the systematic optimization of geometry, topology and material combinations to achieve tailored performance for specific loading histories and reuse requirements.

CRediT authorship contribution statement

Peng-Xu Lu: Methodology, Validation, Writing - Original Draft. **James Dear**: Investigation, Data Curation. **Clare Burnett**: Conceptualization, Investigation. **Jin Zhou**: Conceptualization, Investigation, Data Curation, Supervision, Funding acquisition. **Zhongwei Guan**: Writing - Review & Editing, Supervision. **Zafer Kazancı**: Conceptualization, Investigation, Supervision. **John P. Dear**: Writing - Review & Editing, Supervision.

Declaration of conflicting of interest

The authors declare no potential conflicts of interest with respect to the research, authorship, and/or publication of this article.

Acknowledgment

The strong technical support, for this research, in the State Key Laboratory for Manufacturing Systems Engineering, at Xi'an Jiaotong University, is very much appreciated.

References

[1] Zhang Q, Yang X, Li P, Huang G, Feng S, Shen C, et al. Bioinspired engineering of honeycomb structure – Using nature to inspire human innovation. Prog. Mater. Sci. 2015;74:332-400.

[2] Schaedler TA, Carter WB. Architected Cellular Materials. Annu. Rev. Mater. Res. 2016;46(1):187-210.

[3] Qi C, Jiang F, Yang S. Advanced honeycomb designs for improving mechanical properties: A review. Compos. Part B-Eng. 2021;227:109393.

[4] Ha NS, Lu G. A review of recent research on bio-inspired structures and materials for energy absorption applications. Compos. Part B-Eng. 2020;181:107496.

[5] Zhang J, Lu G, You Z. Large deformation and energy absorption of additively manufactured auxetic materials and structures: A review. Compos. Part B-Eng. 2020;201:108340.

[6] Wang AJ, McDowell DL. In-Plane Stiffness and Yield Strength of Periodic Metal Honeycombs. J. Eng. Mater. Technol. 2004;126(2):137-56.

[7] Liu Y, Zhang X-C. The influence of cell micro-topology on the in-plane dynamic crushing of honeycombs. Int. J. Impact Eng. 2009;36(1):98-109.

[8] Wang Z, Liu J, Yao S. On folding mechanics of multi-cell thin-walled square tubes. Compos. Part B-Eng. 2018;132:17-27.

[9] Ruan D, Lu G, Wang B, Yu TX. In-plane dynamic crushing of honeycombs—a finite element study. Int. J. Impact Eng. 2003;28(2):161-82.

[10] Hu LL, Yu TX. Dynamic crushing strength of hexagonal honeycombs. Int. J. Impact Eng. 2010;37(5):467-74.

[11] Sun D, Zhang W, Zhao Y, Li G, Xing Y, Gong G. In-plane crushing and energy absorption performance of multi-layer regularly arranged circular honeycombs. Compos. Struct. 2013;96:726-35.

[12] Hu LL, Zhou MZ, Deng H. Dynamic crushing response of auxetic honeycombs under large deformation: Theoretical analysis and numerical simulation. Thin-Walled Struct. 2018;131:373-84.

[13] Wang H, Lu Z, Yang Z, Li X. A novel re-entrant auxetic honeycomb with enhanced in-plane impact resistance. Compos. Struct. 2019;208:758-70.

[14] Qiao JX, Chen CQ. Impact resistance of uniform and functionally graded auxetic double arrowhead honeycombs. Int. J. Impact Eng. 2015;83:47-58.

[15] Zhao X, Gao Q, Wang L, Yu Q, Ma ZD. Dynamic crushing of double-arrowed auxetic structure under impact loading.

Mater. Des. 2018;160:527-37.

[16] Mousanezhad D, Haghpanah B, Ghosh R, Hamouda AM, Nayeb-Hashemi H, Vaziri A. Elastic properties of chiral, anti-chiral, and hierarchical honeycombs: A simple energy-based approach. Theor. Appl. Mech. Lett. 2016;6(2):81-96.

[17] Qi C, Jiang F, Yu C, Yang S. In-plane crushing response of tetra-chiral honeycombs. Int. J. Impact. Eng. 2019;130:247-65.

[18] Wei L, Zhu G, He J, Xu S, Zhao X, Zhao X. A novel star-shaped re-entrant circular auxetic honeycomb to enhance in-plane crushing mechanical properties. Eng. Struct. 2025;337:120565.

[19] Wei L, Zhu G, He J. Improved mixed gradient design method to enhance compression stiffness and energy absorption of auxetic structures. Compos. Struct. 2025;368:119284.

[20] Mohan N, Senthil P, Vinodh S, Jayanth N. A review on composite materials and process parameters optimisation for the fused deposition modelling process. Virtual Phys. Prototy. 2017;12(1):47-59.

[21] Frketic J, Dickens T, Ramakrishnan S. Automated manufacturing and processing of fiber-reinforced polymer (FRP) composites: An additive review of contemporary and modern techniques for advanced materials manufacturing. Addit. Manuf. 2017;14:69-86.

[22] Goh GD, Yap YL, Agarwala S, Yeong WY. Recent Progress in Additive Manufacturing of Fiber Reinforced Polymer Composite. Adv. Mater. Technol. 2018;4(1):1800271.

[23] Sugiyama K, Matsuzaki R, Ueda M, Todoroki A, Hirano Y. 3D printing of composite sandwich structures using continuous carbon fiber and fiber tension. Compos. Part A-APPL. 2018;113:114-21.

[24] Dou H, Ye W, Zhang D, Cheng Y, Huang K, Yang F, Rudykh S. Research on drop-weight impact of continuous carbon fiber reinforced 3D printed honeycomb structure. Mater. Today Commun. 2021;29:102869.

[25] Morales U, Esnaola A, Iragi M, Aretxabaleta L, Aurrekoetxea J. The effect of cross-section geometry on crushing behaviour of 3D printed continuous carbon fibre reinforced polyamide profiles. Compos. Struct. 2021;274:114337.

[26] Quan C, Han B, Hou Z, Zhang Q, Tian X, Lu TJ. 3d printed continuous fiber reinforced composite auxetic honeycomb structures. Compos. Part B-Eng. 2020;187:107858.

[27] Changfang Z, Heow Pueh L, Kheng Lim G, Jianlin Z, Kebin Z, Zhendong Z, et al. Preparation process and compression mechanics of carbon fiber reinforced plastics negative Poisson's ratio structure (CFRP + NPRS). Compos. Struct. 2022;292:115667.

[28] Chikkanna N, Krishnapillai S, Ramachandran V. In-plane and out-of-plane quasi-static compression performance

enhancement of 3D printed re-entrant diamond auxetic metamaterial with geometrical tuning and fiber reinforcement. Def. Technol. 2023;25:1-17.

[29] Zhou J, Liu H, Dear JP, Falzon BG, Kazancı Z. Comparison of different quasi-static loading conditions of additively manufactured composite hexagonal and auxetic cellular structures. Int. J. Mech. Sci. 2023;244:108054.

[30] Farrokhabadi A, Mahdi Ashrafian M, Behravesh AH, Kaveh Hedayati S. Assessment of fiber-reinforcement and foam-filling in the directional energy absorption performance of a 3D printed accordion cellular structure. Compos. Struct. 2022;297:115945.

[31] Chen Y, Ye L, Zhang YX, Fu K. Compression behaviours of 3D-printed CF/PA metamaterials: Experiment and modelling. Int. J. Mech. Sci. 2021;206:106634.

[32] Dou H, Ye W, Zhang D, Cheng Y, Wu C. Comparative study on in-plane compression properties of 3D printed continuous carbon fiber reinforced composite honeycomb and aluminum alloy honeycomb. Thin-Walled Struct. 2022;176:109335.

[33] Pehlivan L, Baykasoğlu C. In-plane crushing behavior and energy absorption of CFRP honeycombs with different core topologies. Thin-Walled Struct. 2024;205:112566.

[34] Chen Y, Jin L. Reusable Energy‐Absorbing Architected Materials Harnessing Snapping‐Back Buckling of Wide Hyperelastic Columns. Adv. Funct. Mater. 2021;31(31):2102113.

[35] Li J, Chen Z, Li Q, Jin L, Zhao Z. Harnessing Friction in Intertwined Structures for High-Capacity Reusable Energy-Absorbing Architected Materials. Adv. Sci. 2022;9(13):e2105769.

[36] Zeng C, Liu L, Bian W, Leng J, Liu Y. Compression behavior and energy absorption of 3D printed continuous fiber reinforced composite honeycomb structures with shape memory effects. Addit. Manuf. 2021;38:101842.

[37] Cheng P, Wang K, Chen X, Le Duigou A, Peng Y, Wen W. Compressive property and shape memory effect of 3D printed continuous ramie fiber reinforced biocomposite corrugated structures. Smart Mater. Struct. 2022;31(12):124003.

[38] Ye W, Dou H, Cheng Y, Zhang D. Self-sensing properties of 3D printed continuous carbon fiber-reinforced PLA/TPU honeycomb structures during cyclic compression. Mater. Lett. 2022;317:132077.

[39] Dong K, Panahi-Sarmad M, Cui Z, Huang X, Xiao X. Electro-induced shape memory effect of 4D printed auxetic composite using PLA/TPU/CNT filament embedded synergistically with continuous carbon fiber: A theoretical & experimental analysis. Compos. Part B-Eng. 2021;220:108994.

[40] Zeng C, Liu L, Bian W, Leng J, Liu Y. Temperature-dependent mechanical response of 4D printed composite lattice

structures reinforced by continuous fiber. Compos. Struct. 2022;280:114952.

[41] Dong K, Wang Y, Wang Z, Qiu W, Zheng P, Xiong Y. Reusability and energy absorption behavior of 4D printed continuous fiber-reinforced auxetic composite structures. Compos. Part A-APPL. 2023;169:107529.

[42] Chen Y, He Q. 3D-printed short carbon fibre reinforced perforated structures with negative Poisson's ratios: Mechanisms and design. Compos. Struct. 2020;236:111859.

[43] Tapia Romero MA, Dehonor Gomez M, Lugo Uribe LE. Prony series calculation for viscoelastic behavior modeling of structural adhesives from DMA data. Ing. Investig. Tecnol. 2020;21(2):1-10.

[44] Liu Y, Zhao C, Xu C, Ren J. Shape recovery effect and energy absorption of reusable honeycomb structures. Compos. Struct. 2025;352:118708.

[45] Liang H, Sun B, Hao W, Sun H, Pu Y, Ma F. Crashworthiness of lantern-like lattice structures with a bidirectional gradient distribution. Int. J. Mech. Sci. 2022;236:107746.

[46] Mohammadi H, Ahmad Z, Petrů M, Mazlan SA, Faizal Johari MA, Hatami H, Rahimian Koloor SS. An insight from nature: honeycomb pattern in advanced structural design for impact energy absorption. J. Mater. Res. Technol. 2023;22:2862-87.

[47] Yin H, Zhang W, Zhu L, Meng F, Liu J, Wen G. Review on lattice structures for energy absorption properties. Compos. Struct. 2023;304:116397.

[48] Wang K, Sun G, Wang J, Yao S, Baghani M, Peng Y. Reversible energy absorbing behaviors of shape-memory thin-walled structures. Eng. Struct. 2023;279:115626.

[49] Chen Y, Cai J, Seyedkanani A, Akbarzadeh A, Cerruti M. Strong and flexible graphene oxide paper for humidity responsive origami metamaterials. Mater. Horiz. 2025.

[50] Lu J, Li Q, Qin R, Wang X, Li T, Niu H, Chen B. Enhanced energy absorption of assembled honeycomb system under in-plane compression. Int. J. Mech. Sci. 2025;299:110404.

[51] Lu P, Zhou J, Liu H, Liu C, Li H, Xing Y, et al. A novel 3D printed self-similar hierarchical re-entrant honeycomb with enhanced energy absorption and shape recoverability. Eng. Struct. 2025;336:120386.

[52] Kaushik V, Kurra S, Adusumalli R. Structure–property relationships in 3D-printed onyx-based composites reinforced with continuous fibers: role of temperature and fiber orientation. Compos. Part C-Open Access 2025;18:100649.

[53] Tang H, Chen Z, Zhou G, Sun X, Li Y, Huang L, et al. Effect of fiber orientation distribution on constant fatigue life diagram of chopped carbon fiber chip-reinforced Sheet Molding Compound (SMC) composite. Int. J. Fatigue.

2019;125:394-405.

[54] Zhu H, Ji C, Wang X, Wang Y, Zhao C, Gao Y, Wang K. A visco-hyperelastic constitutive model with Mullins effect for polyurea under repeated impact load. Int. J. Impact. Eng. 2025;201:105287.

[55] Jiang H, Le Barbenchon L, Bednarcyk BA, Scarpa F, Chen Y. Bioinspired multilayered cellular composites with enhanced energy absorption and shape recovery. Addit. Manuf. 2020;36:101430.

[56] Sahu SK, Badgayan ND, Samanta S, Sahu D, Sreekanth PSR. Influence of cell size on out of plane stiffness and in-plane compliance character of the sandwich beam made with tunable PCTPE nylon honeycomb core and hybrid polymer nanocomposite skin. Int. J. Mech. Sci. 2018;148:284-92.

[57] Gibson LJ, Ashby MF, Schajer GS, Robertson CI. The mechanics of two-dimensional cellular materials. P. R. Soc. A-Math Phy. 1997;382(1782):25-42.

[58] Li W, Jia H, Pu C, Liu X, Xie J. Cell Wall Buckling Mediated Energy Absorption in Lotus-type Porous Copper. J. Mater. Sci. Technol. 2015;31(10):1018-26.

[59] Lu P-X, Wang J, Zhou J, Qiao Z, Cao J, Li H, et al. Investigate the in-plane and out-of-plane elastic properties of spiderweb-inspired hierarchical composite honeycombs using forward analytical and inverse numerical approaches. Eng. Struct. 2026;346:121600.

[60] Cui Y, Zhang J, Lu G, Wang L. Large, plastic deformation behavior of lattice structure in compression. Thin-Walled Struct. 2026;219:114317.

[61] Zhao C, Meng Z, Yi J, Chen CQ. Auxetic metamaterials with double re-entrant configuration. Int. J. Mech. Sci. 2025;301:110505.

[62] Cai J, Seyedkanani A, Shahryari B, Yan Z, Lu P, Orsat V, Akbarzadeh A. Nano-architected GaN spinodoid metamaterials with tailorable anisotropic piezoelectric properties. Mater. Horiz. 2026.

Appendix A

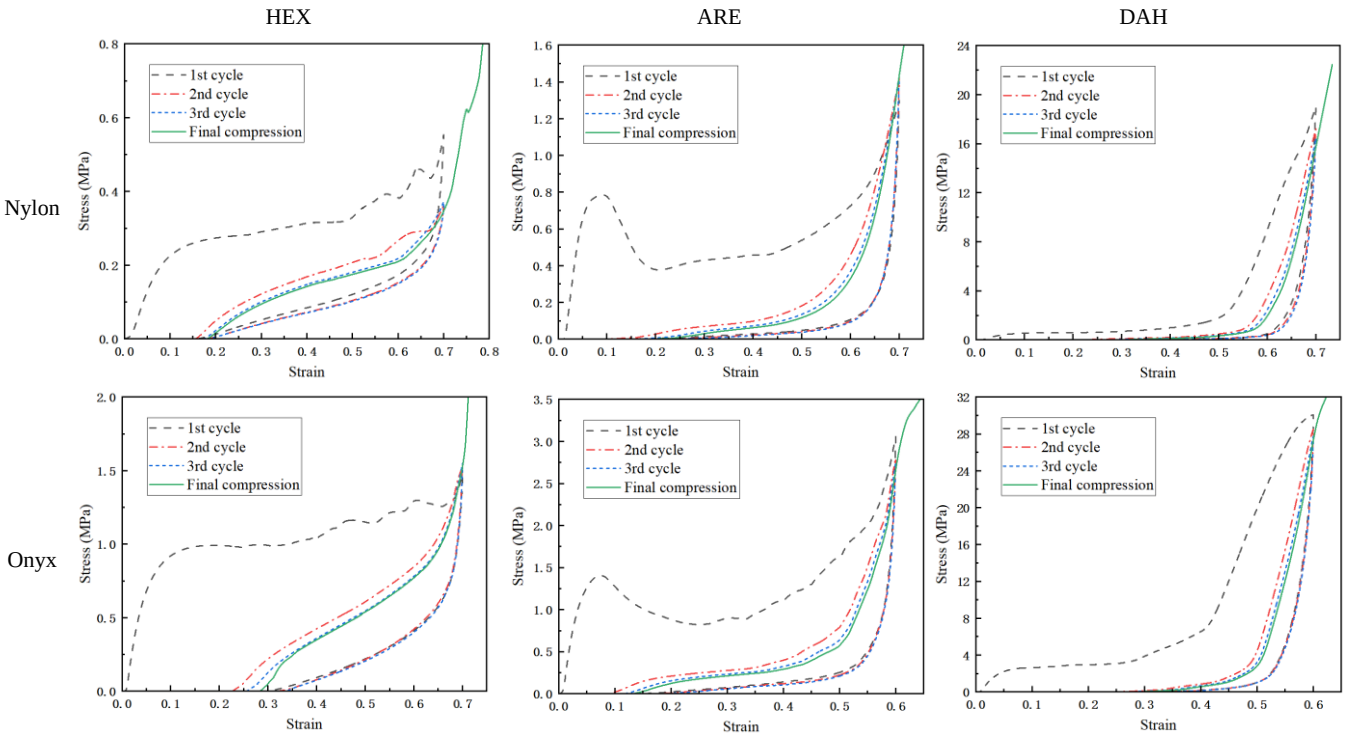


Fig. A.1. The stress-strain curves of honeycombs under cyclic compressions in the transverse direction.

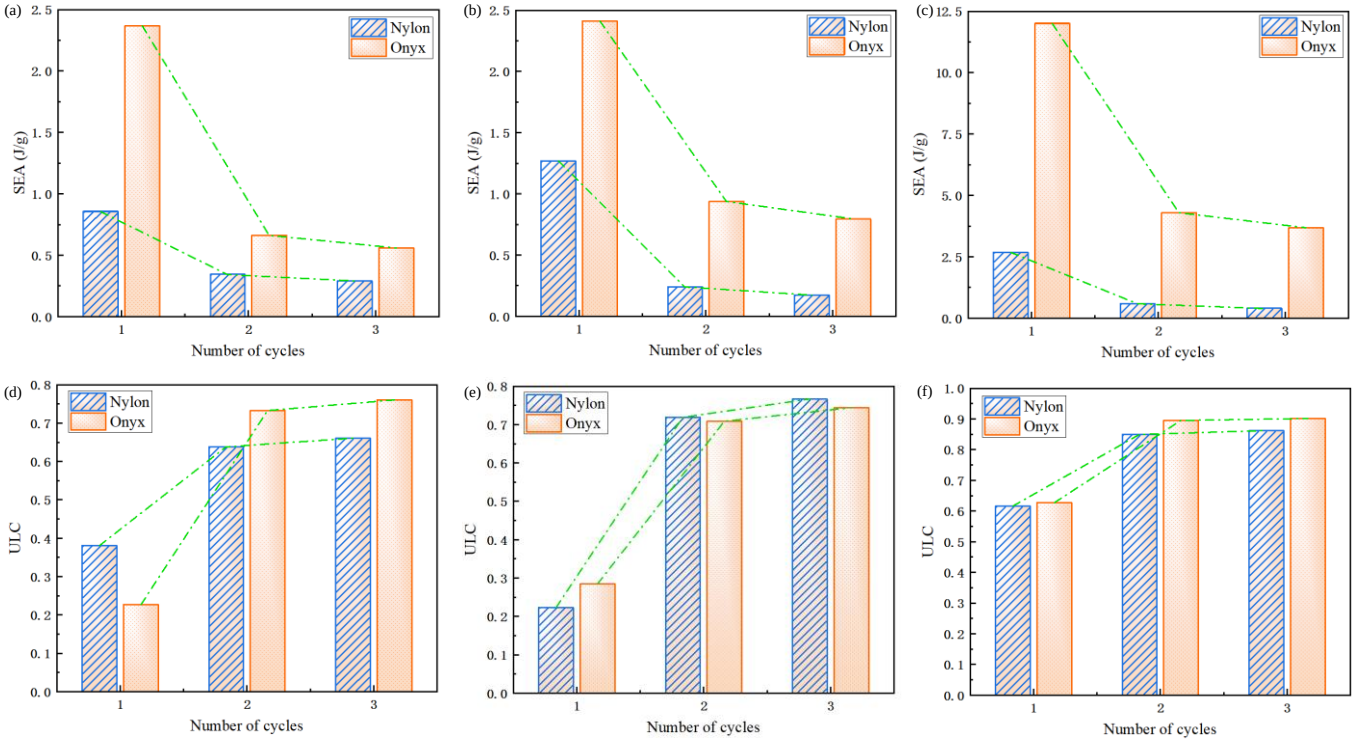


Fig. A.2. Specific Energy Absorption (SEA) of: (a) HEX, (b) ARE, (c) DAH and Undulation of Load-Carrying capacity (ULC) of (d) HEX, (e) ARE, (f) DAH under transverse cyclic loading.

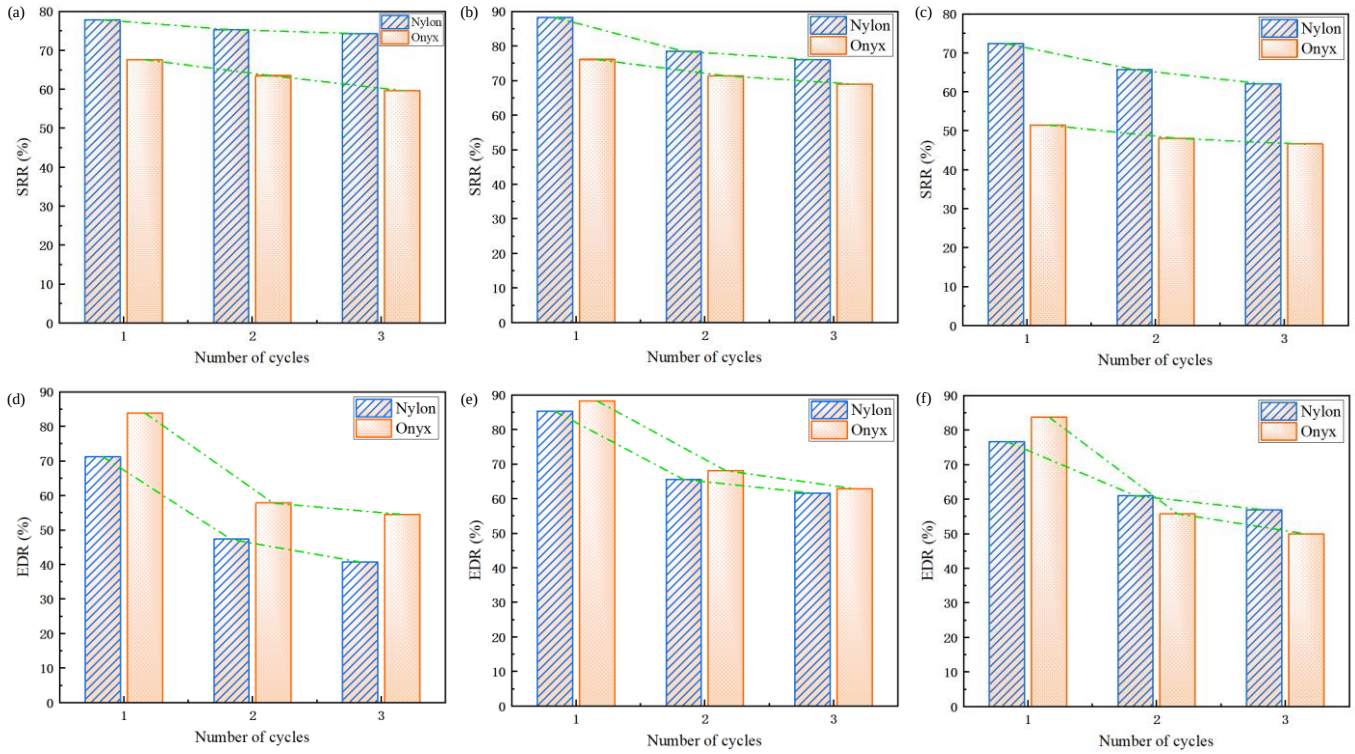


Fig. A.3. Shape Recovery Ratio (SRR) of: (a) HEX, (b) ARE, (c) DAH and Energy Dissipation Ratio (EDR) of: (d) HEX, (e) ARE, (f) DAH under transverse cyclic loading.

Declaration of interests

☒The authors declare that they have no known competing financial interests or personal relationships that could have appeared to influence the work reported in this paper.

☐The authors declare the following financial interests/personal relationships which may be considered as potential competing interests: